J. Fluid Mech. (2025), *vol.* 1010, R3, doi:10.1017/jfm.2025.358

Multi-modal effects on indirect noise induced by turbulent entropy fields

D. Brouzet[1,2], **B. Krisna**[1] **and M. Ihme**[1,3,4]

[1]Department of Mechanical Engineering, Stanford University, Stanford, CA 94305, USA

[2]Center for Turbulence Research, Stanford University, Stanford, CA 94305, USA

[3]Department of Photon Science, SLAC National Accelerator Laboratory, Menlo Park, 94025 CA, USA

[4]Department of Energy Science & Engineering, Stanford University, Stanford, CA 94305, USA

Corresponding author: D. Brouzet, davy.brouzet@gmail.com

(Received 4 November 2024; revised 9 January 2025; accepted 23 March 2025)

Planar entropy waves are commonly assumed for predicting indirect combustion noise. However, the non-planar and turbulent nature of flows found in most practical combustors challenges this assumption. In the present paper, we examine the indirect noise generated by non-planar and turbulent entropy fields through subsonic nozzles. Firstly, we introduce a new transfer function framework that accounts for the contribution of non-planar Fourier modes of the entropy field to the indirect noise spectra. When applied to a turbulent flow field, this method demonstrates a significant improvement in spectral predictions compared with a conventional approach that only considers the planar mode. Secondly, simulations show that non-planar Fourier modes become significant above a threshold frequency f_{thresh}, found in the mid- to high-frequency range. This contribution of non-planar modes is explained by two-dimensional shear effects that distort the entropy waves. A scaling relation that uses residence times along streamlines is developed for f_{thresh}, showing good agreement with simulation results. Finally, we show that the indirect noise from non-planar entropy modes found in aviation combustors can be significant at frequencies below 1 kHz, which might be relevant in situations of thermo-acoustic instabilities coupled to indirect noise.

Key words: aeroacoustics, gas dynamics, stratified turbulence

1. Introduction

The noise generated by aircraft combustors has become a significant contributor to the overall aircraft noise (Ihme 2017). Its significance has been recognised at low-power engine

conditions during landing and approach when the jet exhaust velocity and associated jet noise is low (Ferand *et al.* 2019). Combustion noise is typically divided into direct and indirect contributions. While direct combustion noise arises from pressure fluctuations directly caused by unsteady heat release in the combustion chamber, indirect combustion noise is generated by the acceleration of flow field perturbations when accelerated through the turbine stage or the exit nozzle. Three types of inhomogeneities are responsible for indirect noise, namely compositional noise due to species inhomogeneities (Magri, O'Brien & Ihme 2016; Ihme 2017), vorticity noise due to velocity fluctuations (Cumpsty 1979) and entropy noise due to temperature inhomogeneities (Marble & Candel 1977). The remainder of the paper focuses on the latter.

The first studies on indirect noise assumed one-dimensional (1-D) low-frequency fluctuations to develop the compact nozzle (CN) theory (Marble & Candel 1977). Extension to non-zero frequencies were subsequently performed through, for instance, piecewise linear approximations (Moase, Brear & Manzie 2007) and a Magnus expansion (Duran & Moreau 2013). Many of the more recent investigations have relaxed some of the earlier assumptions, for instance by extending analytical models to compound (Younes & Hickey 2019, 2020) and non-isentropic (De Domenico *et al.* 2019, 2021) nozzles or by considering effects of wall friction (Jain & Magri 2022) and wall heat transfer (Yeddula *et al.* 2022*a*). Past studies have also enhanced our physical understanding of indirect combustion noise. Duran & Moreau (2013) showed that both the modulus and the phase of the transfer functions of subsonic converging–diverging nozzles have a strong dependence on the frequency, leading to a significant decrease in the ratio between indirect and direct noise at high frequencies. This finding complements a model combustor study with the CN approximation from Leyko, Nicoud & Poinsot (2009) who showed that indirect noise can exceed direct noise by an order of magnitude in most realistic aviation combustors. These predictions were confirmed in some combustors through experimental tests (Bake, Michel & Roehle 2007; Miles 2009). Further numerical studies noted that indirect noise exceeded direct noise at low frequencies while being heavily dependent on the operating condition (Shao *et al.* 2022), and could be drastically reduced in next-generation aviation engines that utilise lean premixed combustion (Brouzet *et al.* 2024).

Despite several advancements in modelling and physical understanding, the state-of-the-art methodology for computing indirect noise from turbulent flows solely relies on planar entropy waves, as performed, for instance, in the combustion-generated noise tool CHORUS (Duran *et al.* 2013) or by Tam (2021). Using this approach, Livebardon *et al.* (2016) demonstrated the importance of indirect noise generated in a helicopter engine and Tam (2021) showed that entropy/shock interactions were a significant noise-generating mechanism in a military jet nozzle. Yang, Guzmán-Iñigo & Morgans (2022) and Yeddula *et al.* (2022*b*) are among the few that studied non-planar entropy waves, showing that non-planar effects cause a fall off in the entropy-to-acoustic transfer functions at moderate to high frequencies.

So far, however, it is unclear to what extent the multi-modal nature of turbulent entropy fields impacts indirect noise. In this study, we address this question by (i) developing an analytic framework to study indirect noise generation by non-planar and multi-modal entropy waves and (ii) performing indirect noise simulations of turbulent flows through subsonic nozzles to quantify the contribution of the non-planar entropy modes. Section 2 describes the methodology used for the simulations and the transfer function methodology for multi-modal fields. Section 3 presents the configurations considered in this study while § 4 discusses the computational results. Finally, the conclusions are summarised in § 5.

2. Methodology

2.1. *Linearised Euler equations solver*

The flow field evolution and acoustic propagation are described considering the linearised Euler equations (LEE). In addition, we assume an ideal, calorically perfect gas composed of a single species and an isentropic flow. The LEE system is written as three-dimensional (3-D) unsteady transport equations for the velocity fluctuations $\boldsymbol{u}'$, the pressure fluctuations p' and the entropy fluctuations s'

$$\partial_t \boldsymbol{u}' + \langle \boldsymbol{u} \rangle \cdot \nabla \boldsymbol{u}' = -\boldsymbol{u}' \cdot \nabla \langle \boldsymbol{u} \rangle - \frac{1}{\langle \rho \rangle} \nabla p' - \left(\frac{p'}{\gamma \langle p \rangle} - \frac{s'}{c_p} \right) \langle \boldsymbol{u} \rangle \cdot \nabla \langle \boldsymbol{u} \rangle, \tag{2.1}$$

$$\partial_t p' + \langle \boldsymbol{u} \rangle \cdot \nabla p' = -\boldsymbol{u}' \cdot \nabla \langle p \rangle - \gamma \left(\langle p \rangle \nabla \cdot \boldsymbol{u}' + p' \nabla \cdot \langle \boldsymbol{u} \rangle \right), \tag{2.2}$$

$$\partial_t s' + \langle \boldsymbol{u} \rangle \cdot \nabla s' = -\boldsymbol{u}' \cdot \nabla \langle s \rangle. \tag{2.3}$$

Here ρ is the density, c_p is the heat capacity, γ is the heat capacity ratio, while $\langle \phi \rangle$ and ϕ' represent the Reynolds average and fluctuations of ϕ so that $\phi(t, x, y, z) = \langle \phi \rangle (x, y, z) + \phi'(t, x, y, z)$. The streamwise, transverse and spanwise directions are represented by x, y and z, respectively The numerical solver described in O'Brien *et al.* (2015) is employed to solve (2.1)–(2.3). These equations are spatially discretised using a 4th-order dispersion-relation-preserving (DRP) finite difference scheme, while the time advancement is performed using a 4th-order Runge–Kutta method. To ensure numerical stability, an 8th-order acoustic-optimised explicit filter is utilised at every time step. Walls are treated as slip with no-penetration boundary conditions for $\boldsymbol{u}'$, while Von Neumann boundary conditions imposing a zero normal gradient are used for s' and p'. Characteristic boundary conditions are applied at the inlet and the outlet of the domain. A sponge region is used at the outlet to avoid any significant vorticity or entropy inhomogeneities to exit the domain. This solver has been used to study indirect noise in a realistic gas-turbine combustor (Shao *et al.* 2021, 2022) and indirect noise due to compositional inhomogeneities (Magri *et al.* 2016).

2.2. *Transfer function analysis for multi-modal fields*

The present section discusses the transfer function modelling framework in the context of indirect noise generation. We consider entropy fluctuations s_1' which are accelerated through a turbine stage or nozzle, and which generate an upstream-propagating acoustic wave and a downstream propagating acoustic wave

$$\begin{aligned} \pi^- &= \left[\frac{p'}{(\gamma \langle p \rangle)} - \frac{u'}{\langle c \rangle} \right]_1 \\ \pi^+ &= \left[\frac{p'}{(\gamma \langle p \rangle)} + \frac{u'}{\langle c \rangle} \right]_2 \end{aligned}, \tag{2.4}$$

where c represents the speed of sound.

Here and in the following, subscripts 1 and 2 refer to the inlet plane ($x = x_1$) and outlet plane ($x = x_2$) of the turbine stage or nozzle, respectively. In a quasi-1-D framework, we assume s_1' and $\pi^\pm$ to be a function only of t, implying that these fields are planar. Note that this approach is referred to as quasi-1-D because the flow and sound generation process are still multi-dimensional. Only s_1' and $\pi^\pm$ are assumed planar. With these assumptions, the acoustic transfer functions $H^\pm$ which relate the entropy input to the acoustic outputs are

$$H^\pm(\omega) = \widehat{\pi}^\pm(\omega) / \widehat{s_1'}(\omega), \tag{2.5}$$

where $\widehat{\cdot}$ denotes the Fourier transform in frequency space, and ω represents the angular frequency.

We now relax the assumption of a planar incoming entropy field so that $s_1' = s_1'(t, y, z)$. Note that we still assume planar acoustic waves such that $\pi^{\pm} = \pi^{\pm}(t)$. For ease of comprehension and to simplify the upcoming mathematical derivations, we remove the spanwise dependence such that $s_1' = s_1'(t, y)$. In that case, rewriting (2.5) considering the y-dependence yields

$$\widehat{\pi}^{\pm}(\omega) = \int_{-L_y/2}^{L_y/2} \widehat{s_1'}(\omega, y) H^{\pm}(\omega, y) \mathrm{d}y, \tag{2.6}$$

where the transverse width of the domain at the inlet is L_y. Equation (2.6) can be interpreted as integrating the acoustic contributions of every streamline throughout the width of the domain. However, computing $H^{\pm}(\omega, y)$ through LEE simulations appears to be a challenging task. To obtain a more useful expression for (2.6), we first perform a Fourier mode decomposition of the entropy field s_1' in the y-direction:

$$s_1'(t, y) = \sum_{n=0}^{\infty} A_n(t) \cos\left(\frac{2\pi n y}{L_y}\right) + \sum_{n=1}^{\infty} B_n(t) \sin\left(\frac{2\pi n y}{L_y}\right), \tag{2.7}$$

where the amplitudes of the nth time-dependent symmetric and anti-symmetric modes are denoted by A_n and B_n, respectively. Note that the planar mode is represented by the $n = 0$ term. A temporal Fourier transform of (2.7) yields

$$\widehat{s_1'}(\omega, y) = \sum_{n=0}^{\infty} \widehat{A}_n(\omega) \cos\left(\frac{2\pi n y}{L_y}\right) + \sum_{n=1}^{\infty} \widehat{B}_n(\omega) \sin\left(\frac{2\pi n y}{L_y}\right). \tag{2.8}$$

Combining (2.6) and (2.8), we can express the acoustic outputs as

$$\widehat{\pi}^{\pm}(\omega) = \sum_{n=0}^{\infty} \widehat{A}_n(\omega) H^{\pm}_{A_n}(\omega) + \sum_{n=1}^{\infty} \widehat{B}_n(\omega) H^{\pm}_{B_n}(\omega), \tag{2.9}$$

where

$$H^{\pm}_{A_n}(\omega) = \int_{-L_y/2}^{L_y/2} \cos\left(\frac{2\pi n y}{L_y}\right) H^{\pm}(\omega, y) \mathrm{d}y, \tag{2.10}$$

$$H^{\pm}_{B_n}(\omega) = \int_{-L_y/2}^{L_y/2} \sin\left(\frac{2\pi n y}{L_y}\right) H^{\pm}(\omega, y) \mathrm{d}y. \tag{2.11}$$

The transfer functions for the symmetric and the anti-symmetric entropy modes are denoted by $H^{\pm}_{A_n}$ and $H^{\pm}_{B_n}$, respectively. Equation (2.9) shows that the non-planar Fourier modes contribute independently to the noise generation through their respective transfer functions.

Equation (2.8) is an orthogonal basis decomposition of $\widehat{s_1'}(\omega, y)$, which represents the input entropy field in spectral space. While any orthogonal basis decomposition of $\widehat{s_1'}$ could have been performed, Fourier modes possess a useful feature. Indeed, in the case of symmetric nozzles, such as those studied therein, the anti-symmetric contributions will vanish, as the integral in (2.11) will be zero. For this reason, we only analyse the acoustic contributions of the symmetric modes in the following. In § 4.2, we use this methodology to compute the noise generated by a turbulent flow field and quantify the non-planar contributions. Specifically, to compute $H^{\pm}_{A_n}(\omega)$, we invert (2.9) by considering one mode n at a time.

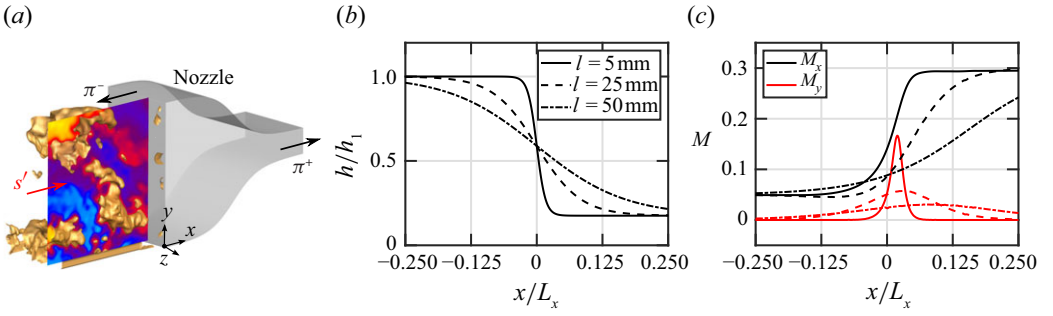

Figure 1. (*a*) Schematic of the configuration considered with (*b*) nozzle height and (*c*) $M_x = \langle u_x \rangle / \langle c \rangle$ and $M_y = \langle u_y \rangle / \langle c \rangle$ for the cases with $l = 5$ mm, 25 mm and 50 mm. Here, M_x and M_y are shown for a streamline starting at $y = 0.95h_1$, close to the nozzle wall. The full length of the nozzle is denoted by L_x.

3. Flow and nozzle configuration

We consider two types of entropy fields: whitenoise signals and a turbulent flow field from a realistic aviation combustor. As shown in figure 1(*a*), these fields are accelerated through an exhaust nozzle, leading to the generation of the $\pi^{\pm}$ acoustic waves.

We refer to whitenoise signals as entropy fields that have equal amplitude over a range of frequencies. These signals result in the superposition of temporal harmonic waves with different frequencies and random phase shifts φ:

$$s_1'(t, y) = \sum_{m=0}^{M} C \sin(m\omega_0 t + \varphi_m) \cos\left(2\pi n y / L_y\right), \tag{3.1}$$

where ω_0 and $M\omega_0$ denote the lowest and highest angular frequencies considered, and $C = 0.01$ is a constant. This approach enables the computation of transfer functions with a single simulation instead of considering several tonal cases. Following the Fourier mode decomposition described in § 2.2, non-planar symmetric modes are also considered by transversely modulating the whitenoise signals with the cosine term in (3.1).

In addition to these whitenoise signals, we also consider a turbulent field from a single injector segment of a realistic gas-turbine combustor to assess non-planar effects in a practical configuration. These results were obtained as part of a previous study (Brouzet *et al.* 2024), where a large-eddy simulation (LES) of a next-generation aviation combustor was performed. This LES reproduced the experimental study of a single sector combustor segment by McCormick, Hultgren & Mendoza (2022). Therefore, potential thermo-acoustic coupling with azimuthal or helical entropy modes are not captured. The combustor features axial staging using separate pilot and main injectors. The pilot injector possesses an air-blast atomiser and creates a non-premixed flame, which anchors the main mixer flame through a reacting jet in crossflow. A take-off condition is considered with a high operating pressure and preheated air. Further details on the configuration, numerical methods, and physics of the combustor can be found in the original study (Brouzet *et al.* 2024). The entropy field downstream of the main flame is used as an inlet to the nozzle described in this section.

A nozzle with a tangent hyperbolic profile is considered, where the nozzle height is defined as $h(x) = 0.5(h_2 + h_1) + 0.5(h_2 - h_1)\tanh(x/l)$, with $-L_x/2 < x < L_x/2$ where $L_x = 300$ mm denotes the full length of the nozzle. The characteristic nozzle length, representative of the constriction rate, is denoted by l. A ratio $h_1/h_2 = 5.7$ is chosen to obtain a subsonic Mach number $M_2 = 0.30$ with $M_1 = 0.05$. Thirty equidistantly

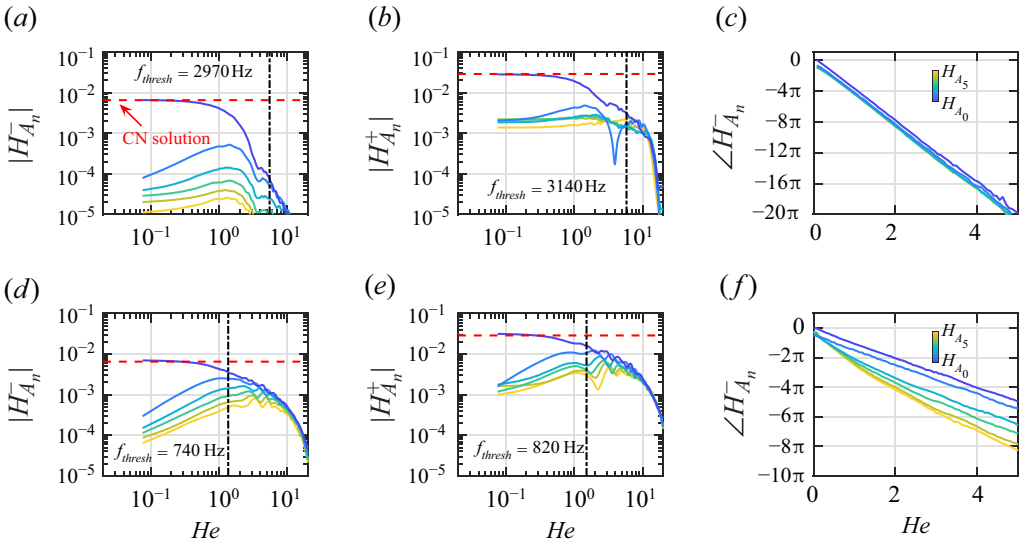

Figure 2. Magnitude of the transfer functions $H^{\pm}_{A_n}$ for the symmetric modes ($n \leqslant 5$) in the (*a,b*) $l = 50$ mm and (*d,e*) $l = 5$ mm nozzles. The phases of $H^-_{A_n}$ are shown for (*c*) $l = 50$ mm and (*f*) $l = 5$ mm. The horizontal dashed lines represent the CN solution and the vertical dot-dashed lines show the threshold frequency f_{thresh} at which the difference between the planar mode and the loudest non-planar mode is less than 3 dB.

spaced numerical probes record p' and u' at the streamwise locations $x = -0.45L_x$ and $x = 0.45L_x$. The p' and u' traces are then ensemble averaged before computing π^- and π^+ with the equations shown in the first paragraph of § 2.2. When studying non-zero frequency effects, the geometry of the nozzle affects the streamwise and transverse velocity profiles and, in turn, the generated indirect noise (Emmanuelli *et al.* 2020; Huet, Emmanuelli & Le Garrec 2020). We therefore consider different nozzles with $l = 5$ mm, 25 mm and 50 mm. The profiles of the nozzles and their flow Mach number are shown in figure 1(*b–c*) as a function of the streamwise coordinate. As the characteristic length of the nozzle decreases, the amplitude of the transverse flow increases. To reduce computational costs and simplify the analysis, the calculations are two-dimensional (2-D), considering only the streamwise and transverse directions, x and y. Therefore, the inlet entropy fluctuations correspond to the spanwise-average of the turbulent field. For all cases, we consider inlet conditions similar to those found in the realistic aviation combustor, with $\langle p_1 \rangle = 2.8$ MPa, $\langle c_1 \rangle = 820$ m s^{-1} and $\gamma = 1.4$. Reynolds average fields necessary to solve (2.1) to (2.3) are computed from Reynolds-averaged Navier–Stokes (RANS) simulations with the commercial software ANSYS.

4. Results

4.1. *Whitenoise entropy fields*

We have performed LEE computations for whitenoise entropy signals with planar and non-planar symmetric modes up to $n = 5$. The magnitude of the transfer functions $H^{\pm}_{A_n}$ for the cases with $l = 50$ mm and $l = 5$ mm are shown in figure 2(*a,b*) and figure 2(*d,e*), respectively, as a function of the convective Helmholtz number $He = fh_1/u_1$. The transfer functions presented in this study have been filtered over a 1/12-octave band for improved convergence at high frequencies. The results from the CN theory are also displayed, showing good agreement with $H^{\pm}_{A_0}$ at low frequencies.

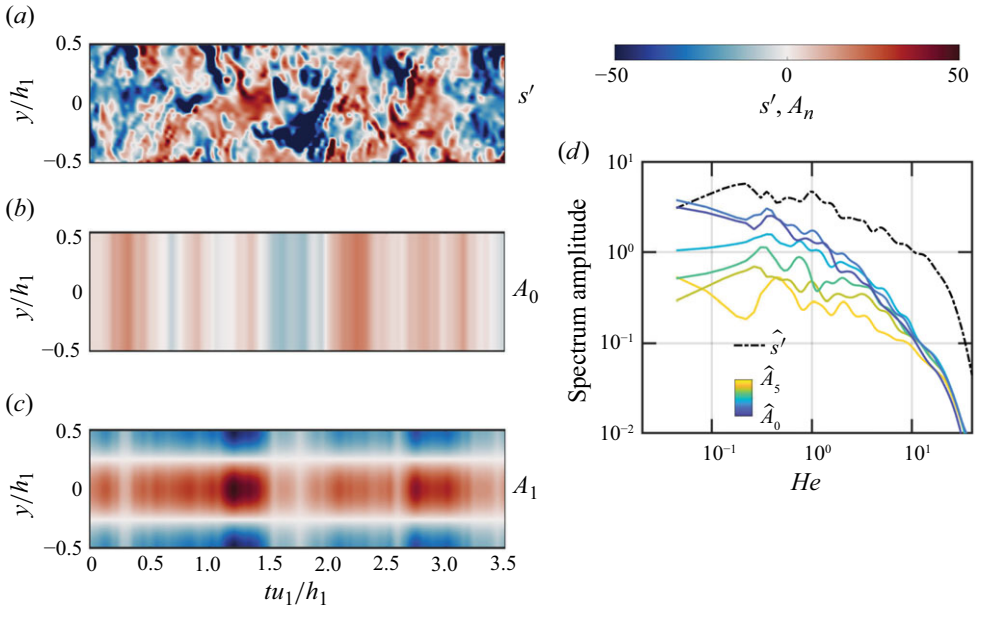

Figure 3. (*a*) Turbulent entropy field from Brouzet *et al.* (2024) with (*b*) planar mode A_0 and (*c*) non-planar mode A_1. The corresponding spectra are shown in (*d*).

In the low-frequency range, the non-planar modes are at least an order of magnitude smaller in amplitude, which corresponds to a relative difference of 20 dB or more. The vertical dot-dashed lines represent the frequency f_{thresh} at which the difference between the loudest non-planar mode and the planar mode is less than 3 dB. This frequency therefore indicates when the non-planar modes become acoustically significant. As the characteristic length of the nozzle decreases, f_{thresh} decreases and the amplitude of the non-planar modes approaches the CN solution. Specifically, the $n = 1$ mode in figure 2(*e*) reaches an amplitude corresponding to 35 % of the CN solution at 370 Hz (or $He = 0.68$), showing the relevance of non-planar modes for indirect noise at intermediate frequencies. Note that minor acoustic reflections are expected at the inlet due to the injection of non-planar waves. As discussed in the supplementary material (available at https://doi.org/10.1017/jfm.2025.358), however, these reflections are not expected to significantly affect the results presented in this paper.

Figure 2(*c*,*f*) show the phases of the $H^-_{A_n}$ transfer functions for the two nozzles considered. The results for $H^+_{A_n}$ are similar and not shown for the sake of brevity. With $l = 50$ mm, the phases are linear for all modes up to $n = 5$ in the frequency range of interest. This means that the finite spatial extent of the nozzle causes a constant time delay in the acoustic wave response regardless of the transverse nature of the entropy field. However, the phases of the $n \geqslant 2$ modes have a nonlinear behaviour in the $l = 5$ mm nozzle, showing that the indirect noise generated by non-planar modes can be drastically affected by the transverse flow.

4.2. *Turbulent entropy field*

In § 2.2, we have established that the indirect noise generated by a multi-modal entropy field can be computed by considering its different spatial Fourier modes independently. This strategy is now applied to the turbulent field described in § 3. Figure 3(*a*) shows

the entropy fluctuations s_1' obtained at a probe located in the downstream section of the aviation combustor studied by Brouzet *et al.* (2024). The corresponding planar mode A_0 and first non-planar mode A_1 are displayed in figures 3(*b*) and (*c*), respectively. The amplitude of A_0 is noticeably smaller than s_1' due to the cancellation between positive and negative fluctuations when performing spatial averaging in the transverse direction. Furthermore, A_1 appears to have a greater magnitude than A_0, indicating stratification of the flow field. Such stratification is commonly found in aviation combustors, especially when dilution and/or effusion cooling is employed (Blomeyer *et al.* 1999; Shao *et al.* 2022).

For a quantitative analysis, figure 3(*d*) shows the spectra of s_1' (dot-dashed line) and all modes A_n for $n \leqslant 5$ (solid lines) as a function of He. The spectra have been filtered over a 1/3-octave band, as oscillations were present when using narrower band filtering, which introduced variations in the uncertainties but did not change the results quantitatively. While the spectra for A_0 and A_1 are similar, the modes become less significant as n increases. The s_1' spectrum features turbulence characteristics: monotonous decay with increasing frequency, power-law dependence in the inertial range, and exponential decay in the dissipation range. The A_0 mode spectrum has a smaller amplitude at all frequencies, consistent with figure 3(*a,b*), and does not possess the same power-law decay in the inertial range. This discrepancy highlights the necessity of using the relevant turbulent entropy spectrum associated with the modes A_n when computing indirect noise through a transfer function approach. With the turbulent flow considered in figure 3, an over-prediction of 10 dB would be observed at $He = 1$ if s_1' was used instead of the planar mode fluctuations A_0. This result has direct implications for the experimental investigation of indirect noise since a single probe measurement is not sufficient to compute a planar or non-planar mode spectrum. Computational approaches could provide additional information and could be used to quantify combustor exit mode shapes.

With the transfer functions $H^{\pm}_{A_n}$ (figure 2) and the entropy spectra $\widehat{A}_n$ (figure 3), we can now compute the acoustic waves $\pi^{\pm}$ by simplifying (2.9) and truncating the summation as

$$\widehat{\pi}^{\pm}_N = \sum_{n=0}^{N} H^{\pm}_{A_n} \widehat{A}_n. \tag{4.1}$$

Specifically, we compute $\widehat{\pi}^{\pm}_0$, i.e. using only the planar mode, and $\widehat{\pi}^{\pm}_5$, i.e. adding the contributions of the first five non-planar symmetric modes. Figure 4 compares $\widehat{\pi}^{\pm}_0$ and $\widehat{\pi}^{\pm}_5$ with the prediction from the LEE simulations ($\widehat{\pi}^{\pm}_{LEE}$) for the $l = 50$ mm (panels (*a–c*)) and $l = 5$ mm (panels (*d–f*)) nozzles. First, the planar mode prediction $\pi^{\pm}_0$ fails at mid to high frequencies, when the contribution from the non-planar modes becomes significant. The vertical lines represent the frequency f_{thresh} at which the difference between $\widehat{\pi}^{\pm}_{LEE}$ and $\widehat{\pi}^{\pm}_0$ exceeds 3 dB. As for the transfer functions, f_{thresh} decreases when the nozzle becomes more compact, confirming that non-planar modes can be acoustically significant at frequencies below 1 kHz. The $\widehat{\pi}^{\pm}_5$ spectra show a better agreement with the LEE results in this mid- to high-frequency range. To better quantify the performance of the two spectra computed via the transfer function approach, we report the differences $\Delta^{\pm}_0 = \pi^{\pm}_0 - \pi^{\pm}_{LEE}$ and $\Delta^{\pm}_5 = \pi^{\pm}_5 - \pi^{\pm}_{LEE}$ as a function of He in figure 4(*c,f*). While the model considering non-planar modes performs significantly better only at high frequencies (>3 kHz) for the $l = 50$ mm nozzle, smaller $\Delta^{\pm}_5$ values are observed around 1 kHz with $l = 5$ mm. Overall, considering non-planar modes in the transfer function formulation significantly improves the prediction of the noise spectra generated by turbulent flow fields. Further

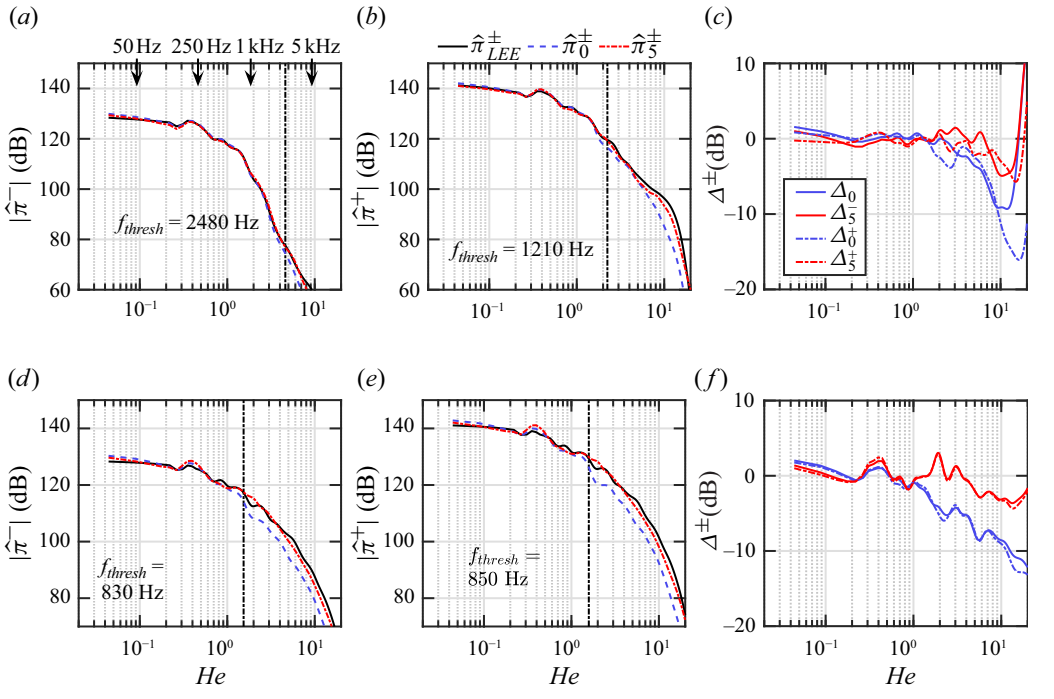

Figure 4. Spectra of $\pi^{\pm}_{LEE}$ (solid lines), $\pi^{\pm}_{0}$ (dashed lines) and $\pi^{\pm}_{5}$ (dot-dashed lines) for the (*a,d*) $\hat{\pi}^{-}$ and (*b,e*) $\hat{\pi}^{+}$ acoustic waves. Panels (*c,f*) show $\Delta^{\pm}_{0}$ and $\Delta^{\pm}_{5}$. Results for the $l = 50$ mm (*a–c*) and $l = 5$ mm (*d–f*) nozzles are shown.

improvements in the acoustic wave prediction at high frequencies could be obtained by considering modes A_n for $n > 5$.

4.3. *Scaling relation for* f_{thresh}

We use scaling analysis to estimate dependencies of f_{thresh} and identify the frequencies at which non-planar waves become significant for a given nozzle geometry. To provide a phenomenological understanding and scaling, we show in figure 5(*a*) a schematic of the nozzle with two streamlines, one at the centreline and one close to the nozzle's wall. Positive and negative entropy contributions are depicted by + and − circles. At the inlet of the nozzle, the positive and negative entropy contributions cancel each other when a transverse integration is performed. As the entropy fluctuations are convected by the mean flow, the shear will distort the original shape of the wave, leading to a different acoustic response compared with a quasi-1-D flow. Specifically, shear will induce a difference in resident times τ between streamlines. An associated phase difference $\Delta\phi$ can be computed as

$$\Delta\phi = 2\pi f \tau. \tag{4.2}$$

If $\Delta\phi$ is of the order of π or larger, as depicted in figure 5, cancellation effects will not occur when a transverse integration is performed, or at least not completely. As a result, the indirect noise generated by non-planar waves will become larger. By rearranging (4.2), we can therefore identify the threshold frequency at which we expect non-planar modes to be acoustically significant:

$$f_{thresh} = \frac{1}{2\tau_{max}}, \tag{4.3}$$

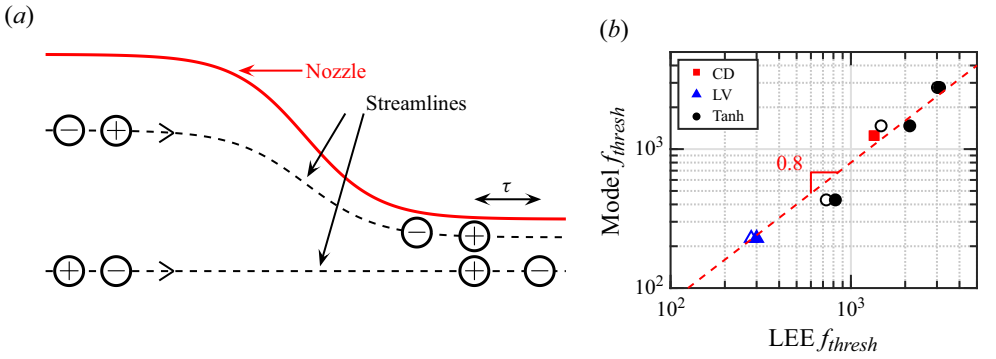

Figure 5. (*a*) Schematic explaining the effect of shear on the non-planar entropy waves. (*b*) Comparison between f_{thresh} obtained with the LEE results and the scaling model (4.3) for a converging–diverging (CD) nozzle, a linear-velocity (LV) nozzle and the tangent-hyperbolic (Tanh) nozzle introduced in § 3. Open and closed symbols represent π^- and π^+ results, respectively.

where τ_{max} represents the maximum resident time difference between two streamlines. Practically speaking, 50 streamlines equidistantly spaced across the nozzle height are first computed based on $\langle u \rangle$. Their residence time from the inlet to the outlet of the nozzle is then computed by integrating $\langle u \rangle$ along the streamline paths. Here, τ_{max} is defined as the difference between the smallest and largest residence times.

Figure 5(*b*) shows the result of the scaling relation (4.3), compared with the results from the LEE. In addition to the nozzles presented in § 3, we consider two additional cases, i.e. a converging–diverging (CD) nozzle and the linear-velocity (LV) nozzle, both presented in the supplementary material. The quantitatively good predictions of the scaling suggest that 2-D shear effects are responsible for significant acoustic contributions of non-planar entropy modes. Furthermore, it shows that a simple streamline computation can provide an estimation of the frequencies at which non-planar modes are expected to be significant.

5. Conclusions

We studied the indirect noise generated by multi-modal, non-planar entropy waves when accelerated through a nozzle by performing LEE computations. The simulations showed that, while the planar mode was acoustically dominant at low frequencies, non-planar modes become significant above a threshold frequency f_{thresh}, found in the mid- to high-frequency range. These contributions from the non-planar modes were explained by 2-D shear effects from the mean flow, which distort the entropy waves. A nozzle with a higher constriction rate will therefore result in non-planar modes contributing to the indirect noise at lower frequencies. A scaling relation that uses the residence time along streamlines was developed for estimating f_{thresh}. Reasonable agreement with LEE computations for several nozzle configurations was obtained.

To compute the indirect noise generated by multi-modal entropy fields, a transfer function methodology that accounts for the contribution of non-planar Fourier modes was developed. The application of this methodology to a turbulent flow field showed a significant improvement in the indirect noise spectra prediction compared with a conventional method that relies only on the planar mode. Furthermore, this study shows that the indirect noise from non-planar entropy modes found in aviation combustors can be significant at frequencies of interest. Using the data of a next-generation aviation combustor (Brouzet *et al.* 2024), the present study shows significant non-planar acoustic

contributions at frequencies below 1 kHz, which can be relevant in situations of thermo-acoustic instabilities coupled to indirect noise. In many industrial combustors, flows can be stratified to even a higher degree, for instance in the presence of dilution and effusion cooling, or can feature strong azimuthal/helical modes. In these cases, the energy content of the non-planar modes might be significantly larger than that of the planar mode, which could lead to even larger acoustic contribution of the non-planar entropy modes.

Supplementary material. Supplementary material is available at https://doi.org/10.1017/jfm.2025.358.

Funding. This work was partially supported by the AeroAcoustics Research Consortium (AARC) under award OAI-AARCS-24125. Information about AARC can be found at https://oai.org/aeroacoustics/.

Declaration of interests. The authors report no conflict of interest.

References

BAKE, F., MICHEL, U. & ROEHLE, I. 2007 Investigation of entropy noise in aero-engine combustors. *J. Engng Gas Turbines Power* **129**, 370–376.

BLOMEYER, M., KRAUTKREMER, B., HENNECKE, D. & DOERR, T. 1999 Mixing zone optimization of a rich-burn/quick-mix/lean-burn combustor. *J. Propul. Power* **15**, 288–295.

BROUZET, D., KRISNA, B., MCCORMICK, D., REIMANN, C.A., MENDOZA, J. & IHME, M. 2024 Analysis of direct and indirect noise in a next-generation aviation gas turbine combustor. *Combust. Flame* **260**, 113249.

CUMPSTY, N.A. 1979 Jet engine combustion noise: pressure, entropy and vorticity perturbations by unsteady combustion or heat addition. *J. Sound Vib.* **66**, 527–544.

DE DOMENICO, F., ROLLAND, E. & HOCHGREB, S. 2019 A generalised model for acoustic and entropic transfer function of nozzles with losses. *J. Sound Vib.* **440**, 212–230.

DE DOMENICO, F., ROLLAND, E.O., RODRIGUES, J., MAGRI, L. & HOCHGREB, S. 2021 Compositional and entropy indirect noise generated in subsonic non-isentropic nozzles. *J. Fluid Mech.* **910**, A5.

DURAN, I., LEYKO, M., MOREAU, S., NICOUD, F. & POINSOT, T. 2013 Computing combustion noise by combining large eddy simulations with analytical models for the propagation of waves through turbine blades. *C. R. Mécanique* **341**, 131–140.

DURAN, I. & MOREAU, S. 2013 Solution of the quasi-one-dimensional linearized Euler equations using flow invariants and the Magnus expansion. *J. Fluid Mech.* **723**, 190–231.

EMMANUELLI, A., ZHENG, J., HUET, M., GIAUQUE, A., LE GARREC, T. & DUCRUIX, S. 2020 Description and application of a 2D-axisymmetric model for entropy noise in nozzle flows. *J. Sound Vib.* **472**, 115163.

FERAND, M., LIVEBARDON, T., MOREAU, S. & SANJOSE, M. 2019 Numerical prediction of far-field combustion noise from aeronautical engines. *Acoustics* **1**, 174–198.

HUET, M., EMMANUELLI, A. & LE GARREC, T. 2020 Entropy noise modelling in 2D choked nozzle flows. *J. Sound Vib.* **488**, 115637.

IHME, M. 2017 Combustion and engine-core noise. *Annu. Rev, Fluid Mech.* **49**, 277–310.

JAIN, A. & MAGRI, L. 2022 A physical model for indirect noise in non-isentropic nozzles: transfer functions and stability. *J. Fluid Mech.* **935**, A33.

LEYKO, M., NICOUD, F. & POINSOT, T. 2009 Comparison of direct and indirect combustion noise mechanisms in a model combustor. *AIAA J.* **47**, 2709–2716.

LIVEBARDON, T., MOREAU, S., GICQUEL, L., POINSOT, T. & BOUTY, E. 2016 Combining LES of combustion chamber and an actuator disk theory to predict combustion noise in a helicopter engine. *Combust. Flame* **165**, 272–287.

MAGRI, L., O'BRIEN, J. & IHME, M. 2016 Compositional inhomogeneities as a source of indirect combustion noise. *J. Fluid Mech.* **799**, R4.

MARBLE, F.E. & CANDEL, S. 1977 Acoustic disturbance from gas non-uniformities convected through a nozzle. *J. Sound Vib.* **55**, 225–243.

MCCORMICK, D., HULTGREN, L.S. & MENDOZA, M. 2024 Impact of future low-emissions combustor technology on acoustic scaling laws. *J. Propul. Power* **40**, 806–817.

MILES, J.H. 2009 Time delay analysis of turbofan engine direct and indirect combustion noise sources. *J. Propul. Power* **25**, 218–227.

MOASE, W.H., BREAR, M.J. & MANZIE, C. 2007 The forced response of choked nozzles and supersonic diffusers. *J. Fluid Mech.* **585**, 281–304.

O'Brien, J., Kim, J. & Ihme, M. 2015 Linear analysis of jet-engine core noise based upon high-fidelity combustor and turbine simulations. In *AIAA Paper 2015–1004*. American Institute of Aeronautics and Astronautics.

Shao, C., Brouzet, D., Rock, N. & Ihme, M. 2022 Parametric analysis of core-noise from a realistic gas-turbine combustor for cruise and take-off conditions. *Appl. Energy Combust. Sci.* **9**, 100045.

Shao, C., Maeda, K. & Ihme, M. 2021 Analysis of core-noise contributions in a realistic gas-turbine combustor operated near lean blow-out. *Proc. Combust. Inst.* **38**, 6203–6211.

Tam, C.K.W. 2021 On the generation of entropy noise in a shock containing nozzle of high-performance aircraft at afterburner. *J. Sound Vib.* **512**, 116389.

Yang, D., Guzmán-Iñigo, J. & Morgans, A.S. 2022 Sound generated by axisymmetric non-plane entropy waves passing through flow contractions. *Intl J. Aeroacoust.* **21**, 521–536.

Yeddula, S.R., Guzmán-Iñigo, J. & Morgans, A.S. 2022*a* A solution for the qu*a*si-one-dimensional linearised euler equations with heat transfer. *J. Fluid Mech.* **936**, R3.

Yeddula, S.R., Guzmán-Iñigo, J.G., Morgans, A. & Yang, D. 2022*b* A Magnus-expansion-*b*ased model for the sound generated by non-plane entropy perturbations passing through nozzles. In *AIAA Paper 2022–2977*. American Institute of Aeronautics and Astronautics.

Younes, K. & Hickey, J.P. 2019 Indirect noise prediction in compound, multi-stream nozzle flows. *J. Sound Vib.* **442**, 609–623.

Younes, K. & Hickey, J.P. 2020 Effects of shear layer growth on the indirect noise in compound nozzles. *J. Sound Vib.* **468**, 115090.